energies

MDPI

Article

Preparation of N-, O-, and S-Tri-Doped Biochar through One-Pot Pyrolysis of Poplar and Urea Formaldehyde and Its Enhanced Removal of Tetracycline from Wastewater

Wenran Gao [1], Zixiang Lin [1], Shanshan Yan [1], Yaxuan Gao [1], Hong Zhang [1], Xun Hu [2], Hongqi Sun [3] and Shu Zhang [1,*]

[1] Joint International Research Laboratory of Biomass Energy and Materials, Co-Innovation Center of Efficient Processing and Utilization of Forest Resources, College of Materials Science and Engineering, Nanjing Forestry University, Nanjing 210037, China
[2] School of Material Science and Engineering, University of Jinan, Jinan 250022, China
[3] School of Engineering, Edith Cowan University, 270 Joondalup Drive, Joondalup, WA 6027, Australia
* Correspondence: s.zhang@njfu.edu.cn; Tel.: +86-025-8542-8330

Abstract: In this study, biochar was prepared via hybrid doping of N, O, and S by applying one-pot pyrolysis of poplar wood and S-containing urea formaldehyde at 900 °C. Different doping ratios were adopted, and the contents of O, N, and S were in the ranges of 2.78–5.56%, 2.16–4.92%, and 1.42–4.98%, respectively. This hybrid doping significantly enhanced the efficiency of the removal of tetracycline (40 mg/L) from wastewater to 71.84% in comparison with that attained by using normal poplar biochar (29.45%). The adsorption kinetics and isotherms indicated that the adsorption process was favorable and was dominated by chemisorption instead of physisorption; the dominant adsorption process may be justified by the existence of abundant functional groups. The adsorption capacity was barely related to the surface area (R^2 = 0.478), while it was closely related to the concentration of graphitic N (R^2 = 0.985) because graphitic N enhanced the π–π interactions. The adsorption capacity was also highly related to the proportion of oxidized N and oxidized S owing to hydrogen bonding, which may have overlapped with the contribution of O-containing functional groups. This study presents a simple hybrid doping method for biochar modification and provides fundamental insights into the specific effects of O-, N- and S-containing functional groups on the performance of biochar for tetracycline removal.

Keywords: hybrid doping of N, O, and S; biochar; poplar; adsorption; functional groups; tetracycline

Citation: Gao, W.; Lin, Z.; Yan, S.; Gao, Y.; Zhang, H.; Hu, X.; Sun, H.; Zhang, S. Preparation of N-, O-, and S-Tri-Doped Biochar through One-Pot Pyrolysis of Poplar and Urea Formaldehyde and Its Enhanced Removal of Tetracycline from Wastewater. *Energies* **2022**, *15*, 8081. https://doi.org/10.3390/en15218081

Academic Editor: Ying Xu

Received: 17 September 2022
Accepted: 25 October 2022
Published: 31 October 2022

1. Introduction

Biochar prepared through biomass pyrolysis is a solid carbon-rich material [1]. It has been extensively utilized in many arenas, such as pollutant adsorption, soil remediation, carbon-based catalysts, and energy storage, due to its specific properties [2,3]. Compared with other carbon-based adsorbents, such as activated carbon and carbon nanotubes, biochar has gained extensive attention for its environmental friendliness nature, low price, and versatile structure (e.g., porous structure, aromatic structure, and plentiful functional groups) [4–7]. Moreover, the use of biochar is regarded as a carbon-reduction method since biochar can sequester carbon and will, thus, mitigate the climate change caused by greenhouse gas emissions [8–10]. However, the contaminant removal efficiency of primeval biochar is limited by its undeveloped structure [1]. In previous studies, heteroatom-doped (e.g., N, S, P, F, and B) biochar exhibited an enhanced adsorption capacity that was attributed to its optimized structural characteristics, such as its improved pore structure and many active sites on the surface [11–16]. For instance, Li et al. [1] reported that N-doped activated biochar (N content = 10.41%) prepared at 700 °C showed a higher adsorption of phenol (95.88 mg/g) than that prepared at 600 °C (9.58 mg/g, N content = 8.47%) due to the high

content of graphitic N (i.e., N-G). Feng et al. [11] revealed that biochar that was dual-doped with O and N showed an enhanced absorption of phenols, for which the hydroxyl and pyrrole-N (N-6) groups were responsible. Chen et al. [17] and Guo et al. [18] found that the co-doping of an N atom and S atom could decrease the adsorption energy of biochar via synergistic effects and that the biochar exhibited a high adsorption capacity for Cr(VI) and diethyl phthalate.

Water pollution caused by antibiotics is harmful to humankind and aquatic organisms and is becoming increasingly severe [19–21]. Tetracycline (TC) is a typical broad-spectrum antibiotic with a tetraphenyl structure that has been widely used for its low price and effectiveness in medical uses; it is the most widely consumed antibiotic worldwide [22,23]. However, the metabolic efficiency of TC is relatively low, and most of it is evacuated into the environment via urine and feces [24]. TC exists in water bodies such as surface water, groundwater, and drinking water [25]. In recent studies, adsorption has been suggested as a promising technique for purifying TC-polluted water [26–28] due to its cost effectiveness, ease of operation, high removal efficiency, and the lack of secondary pollution involved [29,30]. However, the contribution of tri-doped biochar with O, N, and S species for TC adsorption remains unknown.

Therefore, this study aims to explore the particular effects of O-, N-, and S-containing functional groups on the performance of biochar in TC adsorption. A one-pot hybrid doping process was carried out through the co-pyrolysis of poplar wood and S-containing urea formaldehyde (UF) using different mixing ratios. Poplar wood is a commonly used raw wood material, and UF is a widely used glue in the artificial board industry (e.g., fiberboard, chipboard, and plywood). In this study, the accumulation of waste poplar and artificial board was addressed by showing the potential applications of the biochar derived from them. The N-, O-, and S-tri-doped biochar samples were systemically characterized by using various techniques, including elemental analysis, X-ray photoelectron spectroscopy (XPS), X-ray diffraction (XRD), Raman spectroscopy, and N_2 adsorption/desorption isotherms. These samples were used for TC adsorption, and the influence of the hybrid doping was evaluated. The adsorption isotherms and kinetics were also determined to investigate the adsorption mechanism. Finally, the intrinsic relationship between the adsorption capacity and hybrid doping was revealed.

2. Experimental Section

2.1. Materials

Analytical-grade TC was acquired from Macklin Biochemical (Shanghai, China). HCl (98%) was purchased from Nanjing Chemical Reagent Co., Ltd. (Nanjing, China). Poplar wood and S-containing UF were provided by local wood-processing plants; their elemental analyses are shown in Table S1. UF, also known as wood glue powder, is usually made from powdered UF resin, a reinforcing and curing agent, and it sometimes contains an extender compound. In this study, the UF that was used was prepared by using $(NH_4)_2SO_4$ as the curing agent and gypsum powder ($CaSO_4 \cdot 2H_2O$) as the extender. This type of UF has a high S content (4.96%) and is cheap, which helps to lower the cost of the prepared biochar and increase the economic benefits. All solutions were prepared with deionized water.

2.2. Preparation of Biochar with Hybrid Doping of N, O, and S

As previously reported [31], to begin with, the poplar wood (150–250 μm) and UF were fully mixed, and the mass ratios of UF were 10%, 30%, and 50%, respectively. The N-, O-, and S-tri-doped biochars were produced through slow pyrolysis of the aforementioned mixture with a tube furnace (YGDL-1200, Shanghai Yuzhi Electromechanical Equipment Co., Ltd., Shanghai, China) at 900 °C. A high pyrolysis temperature (900 °C) was chosen because biochar prepared at high temperatures possesses a high degree of graphitization, which is beneficial for TC adsorption [32]. The biochar also had a low content of O, which helped determine the effect of N- and S-containing functional groups. All of the pyrolysis experiments were started at 25 °C with a heating rate of 10 °C/min (up to 900 °C), a holding

time of 1 h, and a N_2 flow rate of 0.6 L/min. To remove both the ash and the impurities, the biochars were washed using 0.2 M HCl when cooled down. Then the biochars were thoroughly washed with deionized water until the filtrate was neutral, and they were dried at 80 °C. Finally, the N-, O-, and S-tri-doped biochar samples were obtained and denoted as NOS-biochar (also denoted as PUF-10%, PUF-30%, and PUF-50% to indicate the UF mass ratios of 10%, 30%, and 50%, respectively). To further investigate the effect of the N-containing functional groups, N-doped biochar samples produced with 90% poplar and 10% urea were obtained, and they are denoted as PU-10%. Undoped biochar (PBC) was prepared from poplar.

2.3. Characterization of Biochar with Hybrid Doping of N, O, and S

The biochar samples were characterized via the following technologies [31]. Ultimate analysis was conducted using an elemental analyzer (Perkin-Elmer 2400 Series II, PerkinElmer, Waltham, MA, USA). The surface morphology and crystalline structure of the biochars were investigated through scanning electron microscopy (SEM; JSM-7600F, Japan Electronics, Tokyo, Japan), Raman spectrometry (DXR 532, Thermo Scientific, Waltham, MA, USA), and X-ray diffraction (XRD; Ultima IV, Rigaku, Tokyo, Japan). The functional groups of the biochars were determined through Fourier transform infrared (FTIR) spectrometry (Vertex 80V, Bruker, Karlsruhe, Germany). XPS (AXIS Ultra DLD, Kratos, Manchester, UK) was adopted to characterize the surface elemental compositions of the biochars. An autosorb specific surface area analyzer (BSD-PS, BeiShiDe Instrument, Beijing, China) with N_2 as the adsorbate at 77 K was applied to study the Brunauer–Emmett–Teller (BET) surface area and pore size distribution of the biochars.

2.4. Batch TC Adsorption Experiments

To perform the batch adsorption experiments, 0.1 g of biochar was added to 100 mL of TC solution (C_0 = 40 mg/L) and stirred for two days at room temperature (~25 °C). Then, 5 mL of the mixture was acquired and separated using a Millipore filter (0.22-μm). After filtering, the concentration of TC was examined via a UV-visible (UV-Vis) spectrophotometer (UV2600i, Shimadzu, Kyoto, Japan) at 360 nm. The removal efficiency (η) was calculated based on Equation (1):

$$\eta = \frac{C_0 - C_e}{C_0} \times 100\% \quad (1)$$

where C_0 and C_e are the initial and equilibrium TC concentrations (mg/L), respectively.

The adsorption capacity, q_e (mg/g), was obtained with Equation (2) [33]:

$$q_e = \frac{C_0 - C_e}{m} V \quad (2)$$

where V is the volume for the TC solution (L), while m is the weight of the biochar (g).

Separate batches of the adsorption experiments were conducted to obtain kinetic data that fit with the pseudo-first- and pseudo-second-order models. A concentration of 40 mg/L was used as the initial concentration of TC, and the TC-to-biochar ratio was 100 mL/100 mg. The mixtures of biochar and TC were stirred for 1/6, 1/2, 1, 2, 4, 6, 10, 12, 24, 29, 35, 36, and 48 h at ~25 °C. Finally, the residual TC concentrations were examined. The formulas of the pseudo-first- and pseudo-second-order models were:

$$\text{Pseudo-first order}: \ \ln(q_e - q_t) = \ln q_e - k_1 t \quad (3)$$

$$\text{Pseudo-second order}: \ \frac{t}{q_t} = \frac{1}{K_2 q_e^2} + \frac{t}{q_e} \quad (4)$$

where q_e (mg/g) is the amount of TC adsorbed at equilibrium, q_t (mg/g) is the amount of TC adsorbed at time t, and k_1 (min^{-1}) and k_2 ($g{\cdot}mg^{-1}h^{-1}$) are the first- and second-order rate constants, respectively.

Other batches of adsorption experiments were conducted to estimate the adsorption isotherms of TC on the NOS-biochar samples. The other parameters remained the same, but the initial TC concentrations were 5, 10, 20, 40, 60, 80, 100, and 120 mg/L, respectively. The mixtures were stirred for two days. The Langmuir and Freundlich isotherm models were used to estimate the adsorption behavior of TC on biochar; see Equations (5) and (6):

$$\text{Langmuir model}: \ q_e = \frac{q_m k_L C_e}{1 + k_L C_e} \tag{5}$$

$$\text{Freundlich model}: \ q_e = k_F c_e^{\frac{1}{n}} \tag{6}$$

where C_e is the TC equilibrium concentration (mg/L), q_e and q_m are the adsorption capacity (mg/g) and the maximum adsorption capacity (mg/g), K_L (L/mmol) and K_F [(mmol/g)·(L/mmol)$^{1/n}$] are the Langmuir and Freundlich constants, and n is the Freundlich constant that has relation to the adsorption efficiency.

3. Results and Discussion

3.1. Characteristics of Biochar with Hybrid Doping of N, O, and S

Table 1 lists the yields and the proximate and elemental analyses of the biochars. When the mass ratio of UF was increased from 0% to 50%, both the yield (20.6–13.9%) and the ash content (4.09–2.83%) of the NOS-biochar decreased, whereas the volatile content (5.70–9.91%) increased. Furthermore, as the doping ratio increased, the carbon content dropped from 97.65% to 83.24%, whereas the oxygen content gradually increased from 1.09% to 5.56%; sulfur was successfully included, and its content increased significantly from 0.01% to 4.98%. The N content of NOS-biochar also increased considerably from 0.26% to 4.92%. The ratios of H/C (aromaticity) and O/C (polarity) displayed similar trends of rising from 0.0112 to 0.0182 and 0.0112 to 0.0670, respectively. The H/C ratio reflects the organic residues in biochar, and N doping may increase the content of organic matter [19]. The increased H/C ratio indicated more organic matter in the NOS-biochar and a decrease in the aromaticity. Therefore, the NOS-biochar can easily undergo electron exchange with pollutants. The O/C ratio reflects the hydrophilicity of biochar, and the hydrophilicity of the NOS-biochar increased gradually. This meant that the higher UF mixing ratio increased the wettability of the surface of the NOS-biochar, and it may have increased the adsorption capacity [1].

Table 1. Yields and proximate and elemental analyses of biochar samples.

Samples	Yield	Proximate Analysis (wt%, db [a])			Elemental Analysis (wt%, daf [b])						
		Volatile	Fixed Carbon	Ash	C	H	O [c]	N	S	H/C [d]	O/C [d]
PBC [e]	20.6	5.70	90.22	4.09	97.55	1.09	1.09	0.26	0.01	0.1341	0.0084
PU-10% [f]	19.4	7.03	91.13	1.84	91.76	1.14	4.13	2.44	0.53	0.1491	0.0338
PUF-10% [g]	20.6	7.21	88.99	3.81	92.21	1.43	2.78	2.16	1.42	0.1861	0.0226
PUF-30% [g]	17.5	8.98	88.17	2.86	87.01	1.47	4.01	3.98	3.53	0.2027	0.0346
PUF-50% [g]	13.9	9.91	87.26	2.83	83.03	1.51	5.56	4.92	4.98	0.2182	0.0502

[a] Dry basis; [b] dry and ash-free basis; [c] by difference; [d] atomic ratio; [e] PBC means biochar derived from poplar; [f] PU-10% stands for biochar prepared with poplar and urea (10% of urea); [g] PUF-X stands for biochar prepared with poplar and urea formaldehyde with the mass ratios of urea formaldehyde being 10%, 30%, and 50%.

The surface functionalities were characterized by using FTIR spectra; see Figure 1a. The broad bands at approximately 3470 and 3417 cm^{-1} may have been due to the –OH stretching vibrations of hydroxyl functional groups and the –NH_2 stretching mode [34,35]. The weak peaks at 2924 cm^{-1} were due to C–H stretching vibrations [36]. The weak peak at 1631 cm^{-1} was assigned to the aromatic stretching of C–C groups or the stretching of C=O, and the very weak peaks at 1384 and 1101 cm^{-1} were due to CH_3 and alcoholic C–C stretching [37,38]. According to the FTIR spectrum, O- and N-containing functional groups were found in the NOS-biochar samples. The aromatic ring structure was also found in NOS-biochar samples

that had a low aromaticity. TC contains phenol, amine, hydroxyl, and ketone groups [39], which can form π–π interactions with the aromatic ring structure and hydrogen bonds with O- and N-containing functional groups on the surface of biochar.

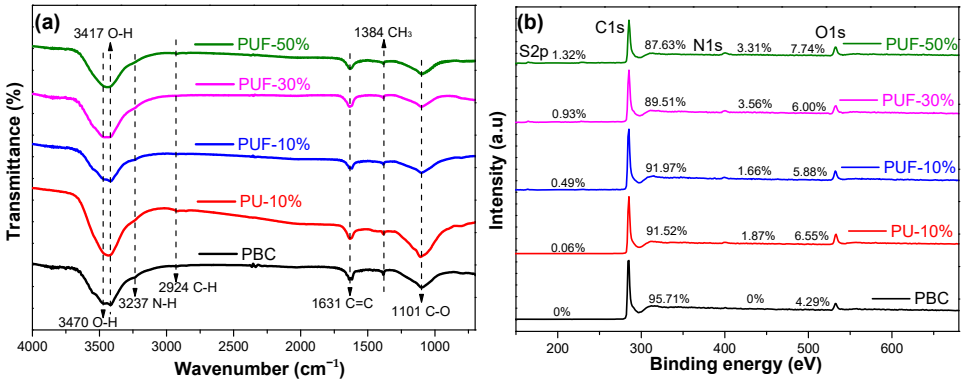

Figure 1. FTIR spectra (**a**) and XPS spectra (**b**) of PBC, PU-10%, PUF-10%, PUF-30%, and PUF-50%. PBC stands for biochar prepared with poplar; PU-10 stands for biochar prepared with poplar and urea, and the mass ratio of urea is 10%; PUF-X stands for biochar prepared with poplar and urea formaldehyde, and the mass ratio of urea formaldehyde is 10%, 30%, or 50%.

To further explore the nature of the surface functionalities, the XPS spectra were investigated. As shown in Figure 1b, four major peaks of C1s, O1s, N1s, and S2p were noticed on the biochar surface, and the atomic contents are listed in Table 2. The C content was reduced when the doping ratio increased, while the N, O, and S contents increased, which was in agreement with the results obtained from the elemental analysis. The highest N and S atomic contents were 3.3 and 1.3 at.%, respectively (PUF-50%).

Table 2. Elemental composition, C-containing functional groups, N-containing functional groups, and S-containing functional groups of the biochar surface from the XPS analysis.

Samples	Elemental Composition (at.%)				Carbon-Containing Functional Group (at.%)			Nitrogen-Containing Functional Group (at.%)				Sulfur-Containing Functional Group (at.%)		
	C	N	O	S	C=C 284.8 eV	C–OH 285.8 eV	C=O 287.2 and 289.2 eV	N-6 398.5 eV	N-5 400.3 eV	N-G 401.2 eV	N-O 403.8 eV	$S2P_{3/2}$ 164.0 eV	$S2P_{1/2}$ 165.2 eV	Sulfate 168.5 eV
PBC	95.71	0	4.29	0	65.5	16.4	18.2	0	0	0	0	0	0	0
PU-10%	91.52	1.87	6.55	0.06	62.7	17.7	19.5	36.7	10.1	26.6	26.5	0	0	0
PUF-10%	91.97	1.66	5.88	0.49	63.2	18.6	18.3	16.5	41.2	23.4	18.9	39.3	32.7	28.0
PUF-30%	89.51	3.56	6.00	0.93	59.6	17.5	22.9	33.4	27.1	18.8	20.8	37.1	46.3	16.5
PUF-50%	87.63	3.31	7.74	1.32	58.1	26.3	15.6	29.9	11.6	30.8	27.7	39.8	20.7	39.5

The peak fittings of C1s, N1s, and S2p are displayed in Figures S1–S3, and the proportion of each element existing in its different forms was calculated according to the results of the peak division (Table 2). The N1s of PBC and the S2p of PBC and PU-10% were not analyzed, as their corresponding contents were lower than the detection limit. The high-resolution S2p peaks of the biochars could be fitted with three peaks that were assigned to oxidized sulfur species (168.5 eV, –C–SO_4–C– or –C–SO_3–C–), as well as $S2p_{1/2}$ (165.2 eV) and $S2p_{3/2}$ (164.0 eV) of the –C–S–C– covalent bond [17,18,40]. The content of oxidized S became larger with a higher doping ratio, while that of tioetheric S fell. The N1s peaks of the NOS-biochar could be fitted into four peaks, which were attributed to pyridinic-N (N-6), pyrrolic-N (N-5), graphitic-N [41], and nitrogen oxides (N-O) [42,43]. The relative content of N-5 dramatically decreased with the increase in the doping ratio, which may have been due to its poor stability, whereas those of N-6, N-G, and N-O rose. Similarly to above, this may have been due to the enhanced reaction between the N- and O-containing groups on the surface of the biochar, which was led by more N-doping [44]. Introducing N-containing and S-containing functional groups could decrease the electronegativity of the C layer. The reduction in the electronegativity improved its adsorption capacity by

increasing its ability to accept π electrons and encouraging the π–π and Lewis acid–base interactions with TC molecules during adsorption [42].

The microscopic morphology of the NOS-biochar with different doping ratios was explored by using SEM (Figure S4). However, the SEM images of the biochar samples with and without N-, O-, and S-tri-doping were very similar, and there was no convincing evidence of the development of a porous structure. To understand the porous structure of the NOS-biochar samples, the N_2 adsorption/desorption isotherms and pore size distribution were analyzed; see Figure 2a. The adsorption isotherms of PBC (undoped biochar), PU-10% (N-doped biochar), and PUF-10% (NOS-biochar with a low doping ratio) had no hysteresis loops and basically met the I-type adsorption isotherm, suggesting the presence of micropore-rich structures. However, when the doping ratio increased, the adsorption isotherm of the NOS-biochar had a visible hysteresis cycle in the relative pressure (P/P_0) range of 0.4–1.0, and it met the IV-type adsorption isotherm, representing the presence of mesopores. The pore size of the biochar samples was predominantly 1.8–2 nm. The BET surface area (see Table 3) was reduced with the addition of 10% UF or urea from 477.1 m^2/g to 431.4 and 459.8 m^2/g, respectively. One possible reason is that the introduction of the N and/or S atoms into the biochar framework may have led to the collapse of microporous passages, which also decreased the total pore volume. However, both the surface area and the pore volume became larger when the doping ratio rose to 30% and 50%. This may be attributed to the pore-forming effect of UF on biochar, as its pyrolysis products are mainly nitrogenous compounds such as isocyanate and NH_3 [45], which can act as activation agents by etching the carbon skeleton during pyrolysis—especially NH_3 [46,47].

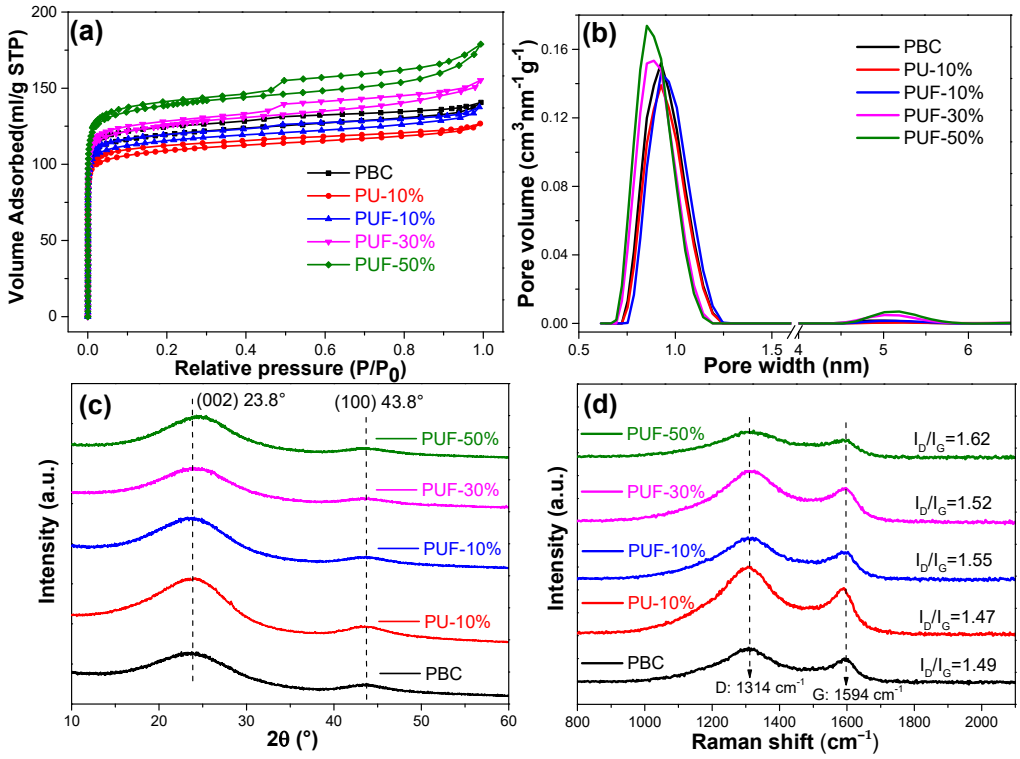

Figure 2. (**a**) Nitrogen adsorption/desorption isotherms, (**b**) pore size distributions, (**c**) XRD patterns, and (**d**) Raman spectra of PBC, PU-10%, PUF-10%, PUF-30%, and PUF-50%.

Table 3. Pore structure of the biochar samples.

Samples	Surface Area (m^2/g)	S_{micro} (m^2/g)	Pore Volume (cm^3/g)	P_{micro} (cm^3/g)	Average Pore Size (nm)
PBC	477.1	440.7	0.216	0.171	1.81
PU-10%	431.4	400.7	0.196	0.157	1.82
PUF-10%	459.8	430.7	0.213	0.168	1.85
PUF-30%	495.4	455.6	0.238	0.180	1.92
PUF-50%	542.5	498.4	0.275	0.198	2.02

The XRD patterns of the biochar samples are displayed in Figure 2c. All samples had similar diffraction peaks that were located at about 24° and 44°, which corresponded to a disordered and amorphous C structure (002) and graphitized C (100) [31]. This aspect suggests that all biochar samples experienced an extent of graphitization crystallization [48,49]. These NOS-biochar and PBC samples had similar diffraction patterns, indicating that atom doping did not significantly alter the overall crystal structure of C. With a higher doping ratio, the (002) peak gradually shifted from 23.8° to 24.5°, meaning that some of the N atoms were introduced into the carbon skeleton. It is known that doping with atoms with a small ionic radius usually leads to a positive shift in the diffraction peak because of the small interlayer space [42].

To investigate the graphitization degree, the Raman spectra of the biochar samples were analyzed; see Figure 2d. The two strong peaks located at 1580 and 1350 cm^{-1} were attributed to the D band, representing a disordered and amorphous structure, and the G band, representing a crystalline graphite structure, which were C sp^2 and sp^2 hybrid configurations, respectively [42]. The relative intensity ratios of D to G (I_D/I_G) were calculated, and the results showed that after N and/or S doping, the I_D/I_G ratio increased from 1.49 to 1.62, suggesting that the degree of graphitization slightly decreased. This indicates that the doping of heteroatoms in C material leads to C disorder and structural defects [50,51]. As mentioned earlier, this occurrence may have been due to the erosion of the biochar by the pyrolysis products of UF. Biochar that contains more defect sites can offer more adsorption sites and, hence, improve the adsorption capacity.

3.2. TC Adsorption Performance of Biochar with Hybrid Doping of N, O, and S

The NOS-biochar samples were applied to remove TC, and the results are presented in Figure 3. The efficiency of TC adsorption by the NOS-biochar was higher than that of PBC (29.45%) and increased from 31.0% to 71.84% with a higher doping ratio. Based on the above discussion on the characterization of biochar samples, there were three reasons for the improvement adsorption performance: (1) The increase in the BET surface area provided more adsorption sites; (2) the increase in the O content provided more O species that could interact with TC molecules via hydrogen bonds; (3) the introduction of N and/or S species enhanced the π–π interaction and Lewis acid–base interaction with the TC molecules. However, the BET surface area of PUF-10% was 459.8 m^2/g and was slightly less than that of PBC (477.1 m^2/g), while the removal efficiency of PUF-10% (31.0%) was a little higher than that of PBC (29.5%). These results imply that the higher content of O, N, and/or S was the main reason for the improvement in the adsorption performance.

To further study the roles of O, N, and S species in TC adsorption, PU-10% with a very low S content was prepared and used to adsorb TC. The results showed that the BET surface area and S content of PU-10% (431 m^2/g and 0.53%) were lower than those of PUF-10%, while the contents of O and N were higher (3.99% and 2.45%). However, the removal efficiency of PU-10% (41.7%) was substantially higher than that of PUF-10%. This suggests that the introduction of N and O into biochar is more important than doping with S species.

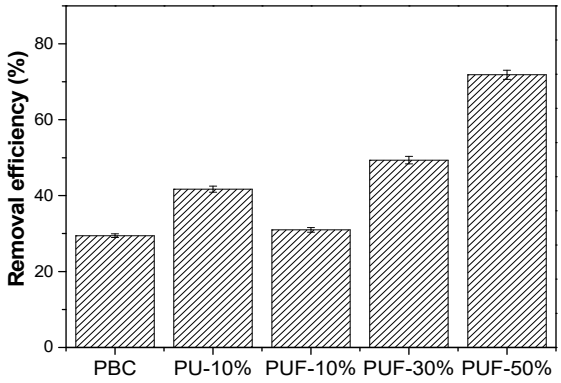

Figure 3. TC removal efficiencies of PBC, PU-10%, PUF-10%, PUF-30%, and PUF-50%.

Adsorption reactions are known to take place on the surface of biochar; thus, it is essential to analyze the elemental composition and functional groups on the surface of biochar. Table 2 shows that PU-10% had slightly higher surface O and N contents than those of PUF-10% and a lower surface S content. This result also implies that, compared to the S-containing functional groups, the O- and N-containing functional groups dominate the TC adsorption ability of biochar. However, this result cannot explain why PUF-50% showed a better adsorption performance than that of PUF-30%, since PUF-30% had a higher surface O content and a slightly lower N content than those of PUF-50%. Therefore, the compositions of different forms of N-containing functional groups were analyzed. Table 2 shows that the proportions of N-5 and N-6 in PUF-30% were higher than those in PUF-50, whereas the proportions of N-G and N-O were lower. PU-10% also possessed higher contents of N-G and N-O than those in PUF-10%. This implies that N-G and N-O play vital roles in the TC adsorption of N-doped biochar among the four types of N-containing functional groups; thus, PUF-50% achieved a greater absorption than PUF-30% did. This is reasonable considering the structure of N-G, in which the N atom is in the middle of three aromatic rings, which leads to a reduction in the electronegativity of the C layer and an improved ability to accept π electrons. As a result, π–π and Lewis acid–base interactions between biochar and TC molecules are encouraged during adsorption, thus improving the adsorption ability of biochar. As for N-O, it can enhance the interactions between TC and biochar through hydrogen bonds.

3.3. Adsorption Isotherms and Kinetics

To evaluate the TC adsorption kinetics of the NOS-biochar, pseudo-first- and pseudo-second-order models were adopted to fit the kinetic adsorption data via linear regression. The adsorption kinetic curves are displayed in Figure 4, and the corresponding fitting parameters are listed in Table 4. The correlation coefficient (R^2) suggests that the pseudo-second-order model (R^2 = 0.95–0.99) fit the kinetic adsorption data better than the pseudo-first-order model did (R^2 = 0.93–0.99). The calculated equilibrium adsorption capacities ($Q_{e,cal}$) of all biochar samples from the pseudo-second-order model were in good agreement with the corresponding experimental data, but those from the pseudo-first-order model varied very much. These facts imply that the behavior of TC adsorption is mainly driven by chemisorption [52,53]. As discussed in Section 3.2, doping with N and/or S generates more functional groups, especially N-containing functional groups, such as N-G and N-O, which offer new chemical adsorption sites [18].

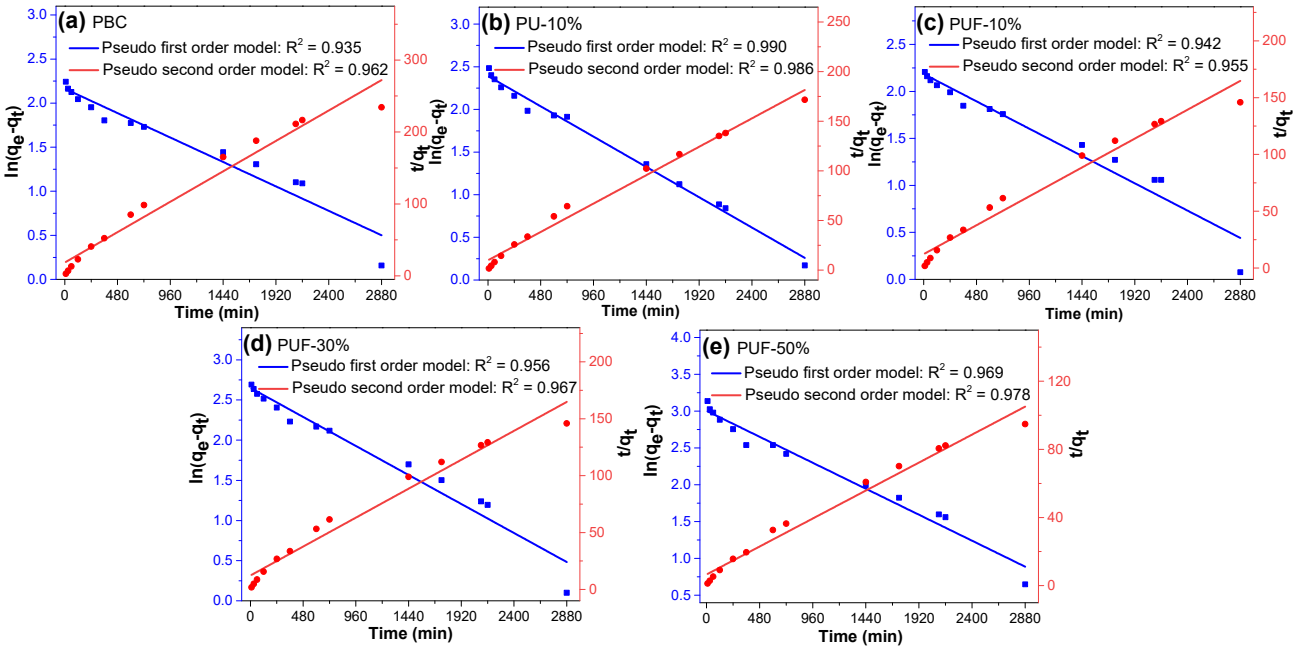

Figure 4. Adsorption kinetics of TC onto (**a**) PBC, (**b**) PU-10%, (**c**) PUF-10%, (**d**) PUF-30%, and (**e**) PUF-50%.

Table 4. Values of the fitting parameters obtained using two models for TC adsorption kinetics.

Samples	Pseudo-First-Order Model			Pseudo-Second-Order Model		
	$Q_{e,cal}$ (mg/g)	K_1 (min^{-1})	R^2	$Q_{e,cal}$ (mg/g)	K_2 (mg/g/min)	R^2
PBC	8.70	5.77×10^{-4}	0.935	11.35	4.21×10^{-4}	0.962
PU-10%	10.93	7.40×10^{-4}	0.990	16.78	3.62×10^{-4}	0.986
PUF-10%	8.88	6.05×10^{-4}	0.942	11.16	3.70×10^{-4}	0.955
PUF-30%	14.16	7.52×10^{-4}	0.956	18.89	0.28×10^{-4}	0.967
PUF-50%	20.17	7.35×10^{-4}	0.969	29.23	1.79×10^{-4}	0.978

The adsorption isotherms were also examined via the Langmuir and Freundlich isotherm models to further study the adsorption mechanisms, and the results are presented in Figure 5 and Table 5. Obviously, the R^2 values of the Freundlich model (0.90–0.95) were larger than those of the Langmuir model (0.80–0.86), suggesting that the Freundlich models better described the behavior of the adsorption of TC onto the hybrid-doped biochar samples. Herein, the adsorption process was more suitable for multilayer adsorption on a heterogeneous surface [54]. The $1/n$ value (heterogeneity factor) was in the range of 0.194–0.346 and was lower than 0.5, which suggested that the adsorption processes were favorable. The dimensionless separation factor, R_L, ranged from 0.23 to 0.47 (which was lower than 1) and proved that the adsorption processes were favorable [32]. Moreover, according to the Langmuir model, a larger doping ratio resulted in a larger q_m value. PUF-50% possessed the highest value of q_m, which was 41.7 mg/g, while PBC possessed the lowest value of q_m (17.4 mg/g). Compared with the values in the literature (Table S2), the adsorption efficiency of the NOS-biochar for TC may be considered to be at an upper-middle level, and it has potential for wastewater treatment even without further activation.

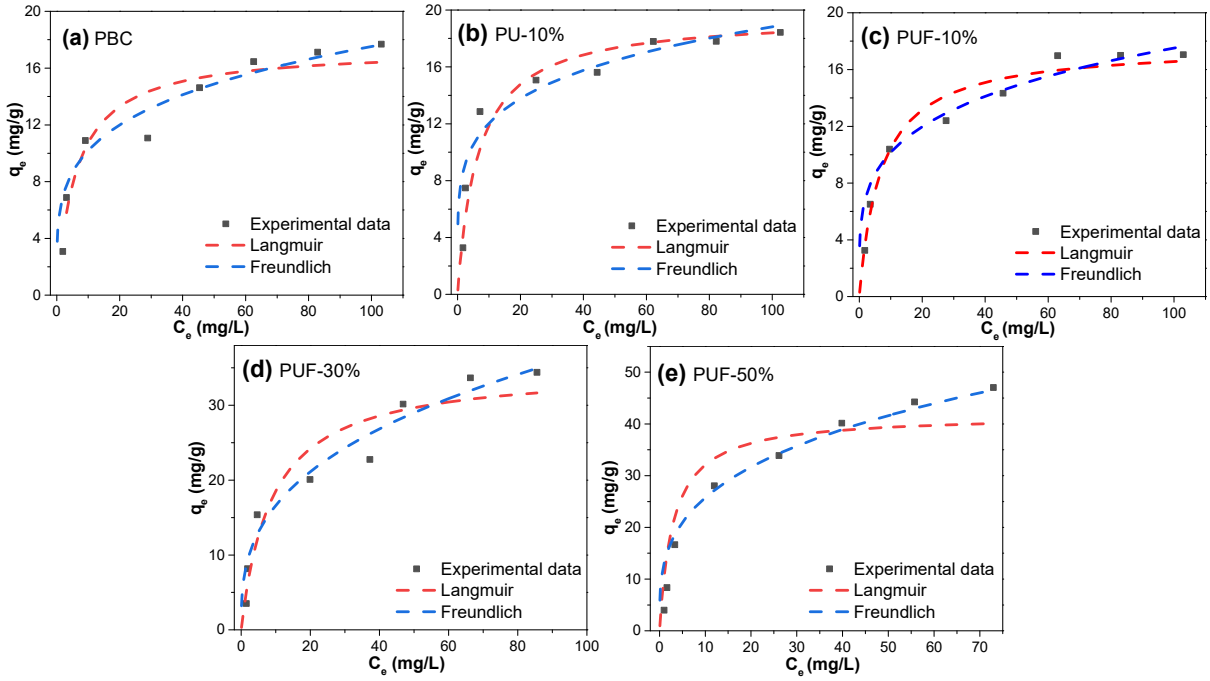

Figure 5. Adsorption isotherms of TC for (**a**) PBC, (**b**) PU-10%, (**c**) PUF-10%, (**d**) PUF-30%, and (**e**) PUF-50%.

Table 5. Langmuir and Freundlich isothermal model parameters for the adsorption of biochar samples onto TC.

Samples	Langmuir Model			Freundlich Model		
	k_L (L/mg)	Q_{max} (mg/g)	R^2	$1/n$	k_F ($mg^{1-n}L^ng^{-1}$)	R^2
PBC	0.1609	17.4	0.810	0.235	5.92	0.936
PU-10%	0.1535	19.6	0.849	0.194	7.70	0.906
PUF-10%	0.1439	17.7	0.805	0.236	5.90	0.943
PUF-30%	0.1129	34.9	0.836	0.350	7.49	0.933
PUF-50%	0.3322	41.7	0.855	0.299	12.94	0.948

3.4. Further Discussion on the TC Adsorption Mechanism

Based on the previous discussion, it may be summarized that the TC adsorption mechanism involved both physical (i.e., pore-filling) and chemical interactions (i.e., electrostatic attraction, Lewis acid–base interactions, hydrogen bonding, and π–π interactions [31]), but the latter prevailed. To further explore the adsorption mechanism, the correlations between the adsorption capacity and relevant biochar properties, including the surface area, elemental content, surface elemental content, and contents of the different kinds of N-containing functional groups, were determined. The results are exhibited in Figures S5–S7, and the corresponding R^2 values are presented in Table S3. The following four aspects may be further discussed.

First, the adsorption capacity was poorly related to the changes in surface area (R^2 = 0.478), indicating that physical effects were unlikely to be the factor that caused the distinctive absorption differences between the samples. The surface areas of the various samples varied between 431.4 and 542.5 m^2/g and did not exhibit dramatic differences. As a result, the chemisorption mechanism was the dominant mechanism.

Second, the correlations between the contents of O, S, and N and the TC adsorption were investigated. Positive correlations existed between TC absorption and the contents of the different elements, with R^2 values of 0.741, 0.635, and 0.847 for O, S, and N, respectively. These results suggest that doping with N and O species has a greater effect on TC absorption, and they are in agreement with the discussions in Section 3.2.

Third, to further explore the effects of the hybrid doping on the absorption performance, the correlations between the surface contents of O, S, and N and the TC absorption were also studied. The surface content of S displayed a considerably higher correlation with TC adsorption (R^2 = 0.882) than that between the overall S content and TC adsorption (R^2 = 0.635). Some oxidized S was able to interact with TC molecules via hydrogen bonds, and their contribution may have overlapped with that of O-containing functional groups. Another interesting observation is that the R^2 of the correlation between the surface content of N and TC adsorption was only 0.385, which was significantly lower than that for the total N content. This may have been due to the varying contributions of the different N-containing functional groups. The R^2 values of N-G, N-6, N-5, and N-O were 0.985, 0.262, 0.444, and 0.882, respectively. These values imply the positive effects of N-G and N-O on TC adsorption and are consistent with the values obtained via the experimental process. This further indicates that π–π interactions may be a vital adsorption mechanism because N-G enhances the ability of C layers to accept π electrons (Section 3.2). Our previous work [31] also suggested that π–π interactions are the main adsorption force and that they result from both the N-G groups and the aromatic structures of biochar. The strong correlation between N-O and the adsorption capacity may also be due to hydrogen bonding, which may also add to the contribution of O-containing functional groups to a certain extent.

4. Conclusions

In this study, biochar was produced via hybrid doping (using different doping ratios) of N, O, and S through pyrolysis of poplar wood and UF at 900 °C. The removal efficiencies for TC (40 mg/L) of PUF-10%, PUF-30%, and PUF-50% were found to be 30.99%, 49.36%, and 71.84%, respectively. These efficiencies were higher than that of PBC (29.45%), which did not undergo heteroatom doping. Further study on PU-10% indicated that the N- and O-containing functional groups played a more crucial role compared to the S-containing functional groups. The adsorption kinetics that were investigated by employing pseudo-first-order and pseudo-second-order models and the adsorption isotherms that were studied by using the Langmuir and Freundlich isotherm models suggested that the adsorption processes were favorable and were dominated by chemisorption instead of physisorption. The functional group analyses and their correlations with the adsorption performance suggested that the hybrid doping successfully enriched multiple O-N and O-S functional groups, as well as N-G groups, all of which were responsible for the improved adsorption performance. In summary, this study presents the utilization of NOS-biochar for the removal of antibiotics from aqueous solutions. Further investigations are encouraged to provide insights into increases in the N content, precise regulation of N-containing functional groups, and the synergistic effects of hybrid doping—especially the synergistic effect with O-containing functional groups.

Supplementary Materials: The following supporting information can be downloaded at: https://www.mdpi.com/article/10.3390/en15218081/s1, Table S1: Elemental analysis of S-containing urea formaldehyde; Table S2: Summary of maximum adsorption capacities (Qmax) of various adsorbents in literature for TC; Table S3: Relationship between selected properties of biochar and adsorption capacity; Figure S1: The C1s spectra of (a) PBC, (b) PU-10%, (c) PUF-10%, (d) PUF-30%, and (e) PUF-50%. PBC stands for biochar prepared by poplar; PU1 stands for biochar prepared by poplar and urea with the mass ratio of urea being 10%; PUF-X stands for biochar prepared by poplar and urea formaldehyde with the mass ratio of urea formaldehyde being 10%, 30% and 50%; Figure S2: The N1s spectra of (a) PU-10%, (b) PUF-10%, (c) PUF-30%, and (d) PUF-50%; Figure S3: The S2p spectra of (a) PUF-10%, (b) PUF-30%, and (c) PUF-50%; Figure S4: SEM images of (a) PBC, (b) PU-10%, (c) PUF-10%, (d) PUF-30%, and (e) PUF-50%; Figure S5: The correlations between surface area of biochar and adsorption capacity; Figure S6: The correlations between (a) oxygen content, (b) sulfur content, (c) nitrogen content, (d) surface oxygen content, (e) surface sulfur content, and (f) surface nitrogen content of biochar and adsorption capacity; Figure S7: The correlations between (a) N-G content, (b) N-6 content, (c) N-5 content, and (d) N-O content of biochar and adsorption capacity. (References [19,24,32,55–58] are cited in the supplementary materials).

Author Contributions: W.G.: Conceptualization, Funding acquisition, Writing—review and editing. Z.L.: Investigation, Data curation, Writing—original draft preparation. S.Y.: Investigation. Y.G.: Investigation. H.Z.: Investigation. X.H.: Investigation. H.S.: Investigation. S.Z.: Supervision, Writing—review and editing. All authors have read and agreed to the published version of the manuscript.

Funding: This research was funded by the Natural Science Foundation of Jiangsu Province (Grant No. BK20200794), National Natural Science Foundation of China (Grant Nos. 52106249 and 51876093), China MOST (Grant No. 2018YFE0183600), and Start-up Fund for Scientific Research of Nanjing Forestry University (Grant No. GXL2020002).

Data Availability Statement: Data available within the article or its Supplementary Materials.

Conflicts of Interest: The authors declare no conflict of interest.

References

1. Li, Y.; Xing, B.; Wang, X.; Wang, K.; Zhu, L.; Wang, S. Nitrogen-doped hierarchical porous biochar derived from corn stalks for phenol-enhanced adsorption. *Energy Fuels* **2019**, *33*, 12459–12468. [CrossRef]
2. Cha, J.S.; Park, S.H.; Jung, S.-C.; Ryu, C.; Jeon, J.-K.; Shin, M.-C.; Park, Y.-K. Production and utilization of biochar: A review. *J. Ind. Eng. Chem.* **2016**, *40*, 1–15. [CrossRef]
3. Wang, T.; Xue, L.; Liu, Y.; Zhang, L.; Xing, B. N self-doped hierarchically porous carbon derived from biomass as an efficient adsorbent for the removal of tetracycline antibiotics. *Sci. Total Environ.* **2022**, *822*, 153567. [CrossRef] [PubMed]
4. Yin, W.; Guo, Z.; Zhao, C.; Xu, J. Removal of Cr(VI) from aqueous media by biochar derived from mixture biomass precursors of *Acorus calamus* Linn. and feather waste. *J. Anal. Appl. Pyrolysis* **2019**, *140*, 86–92. [CrossRef]
5. Hou, Y.; Huang, G.; Li, J.; Yang, Q.; Huang, S.; Cai, J. Hydrothermal conversion of bamboo shoot shell to biochar: Preliminary studies of adsorption equilibrium and kinetics for rhodamine B removal. *J. Anal. Appl. Pyrolysis* **2019**, *143*, 104694. [CrossRef]
6. Song, B.; Cao, X.; Gao, W.; Aziz, S.; Gao, S.; Lam, C.-H.; Lin, R. Preparation of nano-biochar from conventional biorefineries for high-value applications. *Renew. Sustain. Energy Rev.* **2022**, *157*, 112057. [CrossRef]
7. González-Hourcade, M.; Simões dos Reis, G.; Grimm, A.; Dinh, V.M.; Lima, E.C.; Larsson, S.H.; Gentili, F.G. Microalgae biomass as a sustainable precursor to produce nitrogen-doped biochar for efficient removal of emerging pollutants from aqueous media. *J. Clean. Prod.* **2022**, *348*, 131280. [CrossRef]
8. Xu, G.; Han, J.; Ding, B.; Nie, P.; Pan, J.; Dou, H.; Li, H.; Zhang, X. Biomass-derived porous carbon materials with sulfur and nitrogen dual-doping for energy storage. *Green Chem.* **2015**, *17*, 1668–1674. [CrossRef]
9. Yang, G.; Mo, S.; Xing, B.; Dong, J.; Song, X.; Liu, X.; Yuan, J. Effective degradation of phenol via catalytic wet peroxide oxidation over N, S, and Fe-tridoped activated carbon. *Environ. Pollut.* **2020**, *258*, 113687. [CrossRef]
10. Woolf, D.; Amonette, J.E.; Street-Perrott, F.A.; Lehmann, J.; Joseph, S. Sustainable biochar to mitigate global climate change. *Nat. Commun.* **2010**, *1*, 56. [CrossRef]
11. Feng, D.; Guo, D.; Zhang, Y.; Sun, S.; Zhao, Y.; Shang, Q.; Sun, H.; Wu, J.; Tan, H. Functionalized construction of biochar with hierarchical pore structures and surface O-/N-containing groups for phenol adsorption. *Chem. Eng. J.* **2021**, *410*, 127707. [CrossRef]
12. Wang, X.-B.; Yang, S.-Q.; Xu, C.; Ma, H.-D.; Zhang, Z.-H.; Du, Z.-Y.; Li, W.-Y. Effect of boron doping on the performance of Ni/Biochar catalysts for steam reforming of toluene as a tar model compound. *J. Anal. Appl. Pyrolysis* **2021**, *155*, 105033. [CrossRef]
13. Li, Z.; Xing, B.; Ding, Y.; Li, Y.; Wang, S. A high-performance biochar produced from bamboo pyrolysis with in-situ nitrogen doping and activation for adsorption of phenol and methylene blue. *Chin. J. Chem. Eng.* **2020**, *28*, 2872–2880. [CrossRef]
14. Cheng, Y.; Wang, B.; Shen, J.; Yan, P.; Kang, J.; Wang, W.; Bi, L.; Zhu, X.; Li, Y.; Wang, S.; et al. Preparation of novel N-doped biochar and its high adsorption capacity for atrazine based on pi-pi electron donor-acceptor interaction. *J. Hazard. Mater.* **2022**, *432*, 128757. [CrossRef]
15. Dinh, V.C.; Hou, C.H.; Dao, T.N. O, N-doped porous biochar by air oxidation for enhancing heavy metal removal: The role of O, N functional groups. *Chemosphere* **2022**, *293*, 133622. [CrossRef]
16. Zhou, Y.; Tan, P.; He, Z.; Zhang, C.; Fang, Q.; Chen, G. CO_2 adsorption performance of nitrogen-doped porous carbon derived from licorice residue by hydrothermal treatment. *Fuel* **2022**, *311*, 122507. [CrossRef]
17. Chen, F.; Zhang, M.; Ma, L.; Ren, J.; Ma, P.; Li, B.; Wu, N.; Song, Z.; Huang, L. Nitrogen and sulfur codoped micro-mesoporous carbon sheets derived from natural biomass for synergistic removal of chromium(VI): Adsorption behavior and computing mechanism. *Sci. Total Environ.* **2020**, *730*, 138930. [CrossRef]
18. Guo, R.; Yan, L.; Rao, P.; Wang, R.; Guo, X. Nitrogen and sulfur co-doped biochar derived from peanut shell with enhanced adsorption capacity for diethyl phthalate. *Environ. Pollut.* **2020**, *258*, 113674. [CrossRef]
19. Jang, H.M.; Yoo, S.; Choi, Y.K.; Park, S.; Kan, E. Adsorption isotherm, kinetic modeling and mechanism of tetracycline on Pinus taeda-derived activated biochar. *Bioresour. Technol.* **2018**, *259*, 24–31. [CrossRef]
20. Veiga, P.A.d.S.; Schultz, J.; Matos, T.T.d.S.; Fornari, M.R.; Costa, T.G.; Meurer, L.; Mangrich, A.S. Production of high-performance biochar using a simple and low-cost method: Optimization of pyrolysis parameters and evaluation for water treatment. *J. Anal. Appl. Pyrolysis* **2020**, *148*, 104823. [CrossRef]

21. Kasera, N.; Kolar, P.; Hall, S.G. Nitrogen-doped biochars as adsorbents for mitigation of heavy metals and organics from water: A review. *Biochar* **2022**, *4*, 17. [CrossRef]
22. Mei, Y.; Xu, J.; Zhang, Y.; Li, B.; Fan, S.; Xu, H. Effect of Fe-N modification on the properties of biochars and their adsorption behavior on tetracycline removal from aqueous solution. *Bioresour. Technol.* **2021**, *325*, 124732. [CrossRef] [PubMed]
23. Liu, Y.; Li, F.; Deng, J.; Wu, Z.; Lei, T.; Tan, M.; Wu, Z.; Qin, X.; Li, H. Mechanism of sulfamic acid modified biochar for highly efficient removal of tetracycline. *J. Anal. Appl. Pyrolysis* **2021**, *158*, 105247. [CrossRef]
24. Dai, Y.; Li, J.; Shan, D. Adsorption of tetracycline in aqueous solution by biochar derived from waste Auricularia auricula dregs. *Chemosphere* **2020**, *238*, 124432. [CrossRef]
25. Jeong, J.; Song, W.; Cooper, W.J.; Jung, J.; Greaves, J. Degradation of tetracycline antibiotics: Mechanisms and kinetic studies for advanced oxidation/reduction processes. *Chemosphere* **2010**, *78*, 533–540. [CrossRef] [PubMed]
26. Pi, X.; Qu, Z.; Sun, F.; Zhang, Z.; Gao, J. Catalytic activation preparation of nitrogen-doped hierarchical porous bio-char for efficient adsorption of dichloromethane and toluene. *J. Anal. Appl. Pyrolysis* **2021**, *156*, 105150. [CrossRef]
27. Gao, W.; Lin, Z.; Chen, H.; Yan, S.; Huang, Y.; Hu, X.; Zhang, S. A review on N-doped biochar for enhanced water treatment and emerging applications. *Fuel Process. Technol.* **2022**, *237*, 107468. [CrossRef]
28. Li, X.; Xu, J.; Shi, J.; Luo, X. Rapid and efficient adsorption of tetracycline from aqueous solution in a wide pH range by using iron and aminoacetic acid sequentially modified hierarchical porous biochar. *Bioresour. Technol.* **2022**, *346*, 126672. [CrossRef] [PubMed]
29. Li, Y.; Li, Z.; Xing, B.; Li, H.; Ma, Z.; Zhang, W.; Reubroycharoen, P.; Wang, S. Green conversion of bamboo chips into high-performance phenol adsorbent and supercapacitor electrodes by simultaneous activation and nitrogen doping. *J. Anal. Appl. Pyrolysis* **2021**, *155*, 105072. [CrossRef]
30. Qiu, B.; Tao, X.; Wang, H.; Li, W.; Ding, X.; Chu, H. Biochar as a low-cost adsorbent for aqueous heavy metal removal: A review. *J. Anal. Appl. Pyrolysis* **2021**, *155*, 105081. [CrossRef]
31. Gao, W.; Lin, Z.; Chen, H.; Yan, S.; Zhu, H.; Zhang, H.; Sun, H.; Zhang, S.; Zhang, S.; Wu, Y. Roles of graphitization degree and surface functional groups of N-doped activated biochar for phenol adsorption. *J. Anal. Appl. Pyrolysis* **2022**, *167*, 105700. [CrossRef]
32. Xu, D.; Gao, Y.; Lin, Z.; Gao, W.; Zhang, H.; Karnowo, K.; Hu, X.; Sun, H.; Syed-Hassan, S.S.A.; Zhang, S. Application of biochar derived from pyrolysis of waste fiberboard on tetracycline adsorption in aqueous solution. *Front. Chem.* **2019**, *7*, 943. [CrossRef] [PubMed]
33. Hairuddin, M.N.; Mubarak, N.M.; Khalid, M.; Abdullah, E.C.; Walvekar, R.; Karri, R.R. Magnetic palm kernel biochar potential route for phenol removal from wastewater. *Environ. Sci. Pollut. Res. Int.* **2019**, *26*, 35183–35197. [CrossRef]
34. Liu, H.; Dai, P.; Zhang, J.; Zhang, C.; Bao, N.; Cheng, C.; Ren, L. Preparation and evaluation of activated carbons from lotus stalk with trimethyl phosphate and tributyl phosphate activation for lead removal. *Chem. Eng. J.* **2013**, *228*, 425–434. [CrossRef]
35. Wang, L.; Yan, W.; He, C.; Wen, H.; Cai, Z.; Wang, Z.; Chen, Z.; Liu, W. Microwave-assisted preparation of nitrogen-doped biochars by ammonium acetate activation for adsorption of acid red 18. *Appl. Surf. Sci.* **2018**, *433*, 222–231. [CrossRef]
36. Ahmed, M.B.; Zhou, J.L.; Ngo, H.H.; Guo, W.; Chen, M. Progress in the preparation and application of modified biochar for improved contaminant removal from water and wastewater. *Bioresour. Technol.* **2016**, *214*, 836–851. [CrossRef]
37. Li, J.; Wang, L.; Qi, T.; Zhou, Y.; Liu, C.; Chu, J.; Zhang, Y. Different N-containing functional groups modified mesoporous adsorbents for Cr(VI) sequestration: Synthesis, characterization and comparison. *Microporous Mesoporous Mater.* **2008**, *110*, 442–450. [CrossRef]
38. Hamid, S.B.A.; Chowdhury, Z.Z.; Zain, S.M. Base catalytic approach: A promising technique for the activation of biochar for equilibrium sorption studies of copper, Cu(II) Ions in single solute system. *Materials* **2014**, *7*, 2815–2832. [CrossRef]
39. Wei, X.; Zhang, R.; Zhang, W.; Yuan, Y.; Lai, B. High-efficiency adsorption of tetracycline by the prepared waste collagen fiber-derived porous biochar. *RSC Adv.* **2019**, *9*, 39355–39366. [CrossRef]
40. Yan, Y.; Yin, Y.X.; Xin, S.; Guo, Y.G.; Wan, L.J. Ionothermal synthesis of sulfur-doped porous carbons hybridized with graphene as superior anode materials for lithium-ion batteries. *Chem. Commun.* **2012**, *48*, 10663–10665. [CrossRef]
41. Liu, P.; Liu, W.-J.; Jiang, H.; Chen, J.-J.; Li, W.-W.; Yu, H.-Q. Modification of bio-char derived from fast pyrolysis of biomass and its application in removal of tetracycline from aqueous solution. *Bioresour. Technol.* **2012**, *121*, 235–240. [CrossRef] [PubMed]
42. Lian, F.; Cui, G.; Liu, Z.; Duo, L.; Zhang, G.; Xing, B. One-step synthesis of a novel N-doped microporous biochar derived from crop straws with high dye adsorption capacity. *J. Environ. Manag.* **2016**, *176*, 61–68. [CrossRef]
43. Kundu, S.; Xia, W.; Busser, W.; Becker, M.; Schmidt, D.A.; Havenith, M.; Muhler, M. The formation of nitrogen-containing functional groups on carbon nanotube surfaces: A quantitative XPS and TPD study. *Phys. Chem. Chem. Phys.* **2010**, *12*, 4351–4359. [CrossRef]
44. Yu, W.; Lian, F.; Cui, G.; Liu, Z. N-doping effectively enhances the adsorption capacity of biochar for heavy metal ions from aqueous solution. *Chemosphere* **2018**, *193*, 8–16. [CrossRef]
45. Zhu, C.; Cao, J.-P.; Yang, Z.; Zhao, X.-Y.; Yi, W.-C.; Feng, X.-B.; Zhao, Y.-P.; Bai, H.-C. Study on hydrodeoxygenation mechanism of anisole over Ni (111) by first-principles calculation. *Mol. Catal.* **2022**, *523*, 111402. [CrossRef]
46. Girods, P.; Dufour, A.; Rogaume, Y.; Rogaume, C.; Zoulalian, A. Thermal removal of nitrogen species from wood waste containing urea formaldehyde and melamine formaldehyde resins. *J. Hazard. Mater.* **2008**, *159*, 210–221. [CrossRef]
47. Chen, W.; Li, K.; Xia, M.; Chen, Y.; Yang, H.; Chen, Z.; Chen, X.; Chen, H. Influence of NH3 concentration on biomass nitrogen-enriched pyrolysis. *Bioresour. Technol.* **2018**, *263*, 350–357. [CrossRef]
48. Kowalczyk, P.; Deditius, A.; Ela, W.P.; Wiśniewski, M.; Gauden, P.A.; Terzyk, A.P.; Furmaniak, S.; Włoch, J.; Kaneko, K.; Neimark, A.V. Super-sieving effect in phenol adsorption from aqueous solutions on nanoporous carbon beads. *Carbon* **2018**, *135*, 12–20. [CrossRef]

49. Zhang, K.; Sun, P.; Faye, M.C.A.S.; Zhang, Y. Characterization of biochar derived from rice husks and its potential in chlorobenzene degradation. *Carbon* **2018**, *130*, 730–740. [CrossRef]
50. Huang, C.W.; Chiu, S.C.; Lin, W.H.; Li, Y.Y. Preparation and characterization of porous carbon nanofibers from thermal decomposition of poly(ethylene glycol). *J. Phys. Chem. C.* **2008**, *112*, 926–931. [CrossRef]
51. Duan, Q.; Li, X.; Wu, Z.; Alsaedi, A.; Hayat, T.; Chen, C.; Li, J. Adsorption of 17beta-estradiol from aqueous solutions by a novel hierarchically nitrogen-doped porous carbon. *J. Colloid Interface Sci.* **2019**, *533*, 700–708. [CrossRef] [PubMed]
52. Chu, B.; Amano, Y.; Machida, M. Preparation of bean dreg derived N-doped activated carbon with high adsorption for Cr(VI). *Colloids Surf. A Physicochem. Eng. Asp.* **2020**, *586*, 124262. [CrossRef]
53. Tan, K.L.; Hameed, B.H. Insight into the adsorption kinetics models for the removal of contaminants from aqueous solutions. *J. Taiwan Inst. Chem. Eng.* **2017**, *74*, 25–48. [CrossRef]
54. Alizadeh, A.; Abdi, G.; Khodaei, M.M.; Ashokkumar, M.; Amirian, J. Graphene oxide/Fe_3O_4/SO_3H nanohybrid: A new adsorbent for adsorption and reduction of Cr(vi) from aqueous solutions. *RSC Adv.* **2017**, *7*, 14876–14887. [CrossRef]
55. Pouretedal, H.R.; Sadegh, N. Effective removal of Amoxicillin, Cephalexin, Tetracycline and Penicillin G from aqueous solutions using activated carbon nanoparticles prepared from vine wood. *J. Water Process Eng.* **2014**, *1*, 64–73. [CrossRef]
56. Torres-Pérez, J.; Gérente, C.; Andrès, Y. Sustainable Activated Carbons from Agricultural Residues Dedicated to Antibiotic Removal by Adsorption. *Chin. J. Chem. Eng.* **2012**, *20*, 524–529. [CrossRef]
57. Zhu, X.; Liu, Y.; Qian, F.; Zhou, C.; Zhang, S.; Chen, J. Preparation of magnetic porous carbon from waste hydrochar by simultaneous activation and magnetization for tetracycline removal. *Bioresour. Technol.* **2014**, *154*, 209–214. [CrossRef]
58. Wang, H.; Chu, Y.; Fang, C.; Huang, F.; Song, Y.; Xue, X. Sorption of tetracycline on biochar derived from rice straw under different temperatures. *PLoS ONE* **2017**, *12*, e0182776. [CrossRef]